Nucleic Acids Research, 2020 **1**
doi: 10.1093/nar/gkaa634

Type III-A CRISPR-associated protein Csm6 degrades cyclic hexa-adenylate activator using both CARF and HEPN domains

Dalia Smalakyte[1,†], Migle Kazlauskiene[1,†], Jesper F. Havelund[2], Audronė Rukšėnaitė[1], Auguste Rimaite[1], Giedre Tamulaitiene[1], Nils J. Færgeman[2], Gintautas Tamulaitis[1,*] and Virginijus Siksnys[1,*]

[1]Institute of Biotechnology, Vilnius University, Saulėtekio av. 7, LT-10257 Vilnius, Lithuania and [2]Department of Biochemistry and Molecular Biology, VILLUM Center for Bioanalytical Sciences, University of Southern Denmark, Campusvej 55, DK-5230, Odense M, Denmark

Received May 22, 2020; Revised July 12, 2020; Editorial Decision July 14, 2020; Accepted August 06, 2020

ABSTRACT

The type III CRISPR–Cas systems provide immunity against invading nucleic acids through the coordinated transcription-dependent DNA targeting and cyclic adenylate (cA_n)-activated RNA degradation. Here, we show that both these pathways contribute to the *Streptococcus thermophilus* (St) type III-A CRISPR–Cas immunity. HPLC-MS analysis revealed that in the heterologous *Escherichia coli* host the StCsm effector complex predominantly produces cA_5 and cA_6. cA_6 acts as a signaling molecule that binds to the CARF domain of StCsm6 to activate non-specific RNA degradation by the HEPN domain. By dissecting StCsm6 domains we demonstrate that both CARF and HEPN domains act as ring nucleases that degrade cA_ns to switch signaling off. CARF ring nuclease converts cA_6 to linear A_6>p and to the final A_3>p product. HEPN domain, which typically degrades RNA, also shows ring nuclease activity and indiscriminately degrades cA_6 or other cA_ns down to A>p. We propose that concerted action of both ring nucleases enables self-regulation of the RNase activity in the HEPN domain and eliminates all cA_n secondary messengers in the cell when viral infection is combated by a coordinated action of Csm effector and the cA_6-activated Csm6 ribonuclease.

INTRODUCTION

CRISPR–Cas (Clustered Regularly Interspaced Short Palindromic Repeats – CRISPR-associated) adaptive immune systems protect many bacteria and archaea against invading nucleic acids (NAs) such as bacteriophages or plasmids (1). The type III CRISPR–Cas systems provide immunity through the coordinated transcription-dependent DNA targeting and cA_n-dependent RNA degradation pathways. In response to infection, the Csm (type III-A and type-III D) or Cmr (type III-B and III-C) effector complex, guided by the crRNA, binds to the matching sequence in the invading RNA target and activates the Cas10 subunit (2). Activated Cas10 exhibits two different catalytic activities: ssDNase which degrades the target DNA that is being transcribed (3–9) and synthetase which produces cyclic oligoadenylates (cA_ns, $n = 2$–6) that act as secondary messengers (10–15). In addition to *csm* and *cmr* coding genes, *csm6*/*csx*1-like genes are frequently associated with type III CRISPR–Cas systems (16). Csm6 ribonuclease is preferentially associated with type III-A, while Csx1 ribonuclease is found with no clear link to a particular subtype (17,18). We and others have previously shown that cA_6 or cA_4 molecules bind to the CARF (CRISPR-associated Rossmann fold) domain of the Csm6/Csx1 RNases and activate their HEPN (higher eukaryotes and prokaryotes nucleotide-binding) domain for RNA degradation (10–14). Activated Csm6/Csx1 RNases presumably degrade both cellular RNAs and phage transcripts at the later stages of phage infection, which can lead to cell death or dormancy (10,19,20). Some type III systems are predicted to have cA_n binding CARF domains in conjunction with various effector domains such as putative transcription factors or DNases (17,21). The steady state concentration of cA_ns in the cell and the cA_n-dependent Csm6/Csx1 RNase activity depends on two factors: (i) cA_n synthesis that is controlled through target RNA degradation by Csm3 (10,14) and (ii)

*To whom correspondence should be addressed. Tel: +370 5 2234359; Fax: +370 5 2234367; Email: siksnys@ibt.lt
Correspondence may also be addressed to Gintautas Tamulaitis. Tel: +370 5 2234357; Fax: +370 5 2234367; Email: tamulaitis@ibt.lt
†The authors wish it to be known that, in their opinion, the first two authors should be regarded as joint First Authors.
Present address: Migle Kazlauskiene, Department of Biochemistry, University of Zurich, Winterthurerstr. 190, CH-8057 Zurich, Switzerland.

cA_n degradation by specialized enzymes called ring nucleases. A family of ring nucleases composed of a sole CARF domain that degrade cA_4 has been first identified in *Sulfolobus solfataricus* and *Sulfolobus islandicus* (22,23). It has been shown later that the CARF domain of cA_4-dependent Csm6 RNases from *Thermus thermophilus* and *Thermococcus onnurineus* also functions as a ring nuclease that slowly degrades cA_4 (24,25). Recently, a widespread new family of archaeal viral enzymes that efficiently degrade cA_4 has been identified, implying that these enzymes could function as type III anti-CRISPR proteins (26). However, the control and regulation mechanisms of cA_6-dependent CARF RNases remain to be elucidated.

To address this question we have focused on the well-characterized *Streptoccocus thermophilus* type III-A CRISPR–Cas system (8,10,27,28). We have previously shown that *in vitro* StCsm complex produces cA_3, cA_4, cA_5 and cA_6 in decreasing order of abundance and traces of cA_2 (10). Although cA_3 was the major reaction product *in vitro*, the least abundant cA_6 acted as the activator of StCsm6 and StCsm6′ RNases (10), raising a question whether a similar or different set of cA_ns is produced *in vivo*. Using a targeted HPLC-MS analysis of cell metabolites we show here that StCsm complex in the heterologous *E. coli* host produces a range of different cA_ns, with the equilibrium shifted towards cA_5 and cA_6 species. We further show that cells expressing wild type (WT) StCsm6 and StCsm6′ exhibit dramatically lower cA_n levels. Finally, we demonstrate that both CARF and HEPN domains of StCsm6 RNases function as ring nucleases that degrade the cA_6 and other cA_ns to auto-regulate the level of the signaling molecules and to limit the degree of RNA degradation in the cell after phage is eliminated.

MATERIALS AND METHODS

Construction of plasmids

pCas/Csm plasmid carrying genes *cas6*, *cas10*, *csm2*, *csm3*, *csm4*, *csm5*, *csm6′* and *csm6* from *S. thermophilus* DGCC8004 CRISPR2 region (27) and its derivatives was used as a template to generate the following mutant variants: pCas/Csm_dCsm3_dHDCas10, pCas/Csm_dCsm3_dHDCas10_ΔCsm6′ΔCsm6, pCas/Csm_dCsm3_dHDCas10_dPalmCas10_ΔCsm6′ΔCsm6 (see Supplementary Table S1).

To obtain pCas/Csm_dCsm3_dHDCas10, a Cas10(D16A) mutation-containing fragment was PCR amplified from pBAD24_Cas10(D16A)-C-HSH (8) and cloned into pCas/Csm_Csm3(D33A) (27) via SacI and NdeI sites.

To obtain pCas/Csm_dCsm3_dHDCas10_ΔCsm6′ΔCsm6, the constructed pCas/Csm_dCsm3_dHDCas10 was cleaved with PpiI and XmaJI. Sticky ends of the resulting DNA fragment were converted to blunt ends and subjected to ligation. This resulted in the Csm6′ ORF truncation from 386 to 181 codons and elimination of Csm6 ORF.

To obtain pCas/Csm_dCsm3_dHDCas10_dPalmCas10_ΔCsm6′ΔCsm6, a fragment containing Cas10(D575A,D576A) was produced from pBAD24_Cas10(D575A,576A) (8) by PCR. pCas/Csm_dCsm3_dHDCas10_ΔCsm6′ΔCsm6 was digested with AjiI. The resultant vector and PCR fragments were assembled using NEBuilder HiFi DNA Assembly Master Mix (New England Biolabs).

For targeting Tc^R transcript, artificial CRISPR locus was constructed. A synthetic 445 nt CRISPR locus containing four identical 36 nt spacers complementary to the targeted region of the Tc^R RNA separated by four 36 nt repeats and flanked by the leader sequence and the terminal repeat of the *S. thermophilus* DGCC8004 CRISPR2 system was cloned into the pACYC-Duet-1 (Novagen) vector, generating the pCRISPR_Tc plasmid.

pCRISPR_MS2 containing $MS2^{rep}$ spacer flanked by the leader sequence, repeat sequence and a terminal repeat from the *S. thermophilus* DGCC8004 CRISPR2 system was constructed from the pCRISPR_S3 plasmid (27). pCRISPR_S3 was cleaved with XhoI and a fragment containing part of CRISPR locus and two SapI sites was ligated to produce an intermediate plasmid. Further, a fragment containing $MS2^{rep}$ spacer was cloned via SapI site into the intermediate plasmid generating a pCRISPR_MS2 plasmid.

pTarget_$Tc^{handle\ mutant}$ plasmid, a pBR322 derivative having the 3′-flanking region of the Tc target in the Tc^R gene mutated to 5′-CTTTCCGT, was obtained by the QuickChange Mutagenesis (29).

The HEPN domain (172–428 amino acids of StCsm6) expression plasmid pHEPN was constructed in 2 stages. First, to produce an intermediate plasmid, PCR amplified *csm6* gene was cloned into pET-Duet-1 (Novagen) derivative containing an N-terminal His_6-tag and a TEV protease cleavage site coding sequence via Acc65I and AvrII sites. Additional sequence encoding for four Gly residues was introduced between the TEV site and *csm6* by Phusion Site-Directed Mutagenesis (Thermo Fisher Scientific). Finally, inverse PCR cloning (Thermo Fisher Scientific) was used to omit 1–171 codons from *csm6* in the intermediate plasmid.

pdHEPN plasmid containing R371A, H376A mutations in HEPN domain was generated by Phusion Site-Directed Mutagenesis (Thermo Fisher Scientific) using pHEPN as the template.

To generate pCARF plasmid, PCR amplified fragment containing coding sequences of TEV protease cleavage site, four Gly coding sequence, CARF domain (1–169 codons of StCsm6) and PCR fragment obtained from pETDuet-1 (Novagen) derivative containing an N-terminal His_{10}-tag fused with maltose binding protein (MBP) were assembled using NEBuilder HiFi DNA Assembly Master Mix (New England Biolabs). MBP fusion to CARF was used to increase solubility of the CARF domain.

To generate pdCARF and pdCARF-Csm6 plasmids containing D12A mutation in *csm6* gene, mutation carrying primers and pCARF and pCsm6 plasmid (10) as the template, respectively, were used to obtain PCR fragments. These PCR fragments were assembled using NEBuilder HiFi DNA Assembly Master Mix (New England Biolabs).

Protein expression and purification

WT StCsm complex was expressed and purified as described previously (27). Briefly, pCas/Csm plasmid was co-expressed in *E. coli* BL21 (DE3) with pCRISPR_S3, containing four identical spacers S3 interspaced by five repeats of the *S. thermophilus* DGCC8004 CRISPR2 system (27),

and pCsm2N-Tag, encoding the Csm2 gene with an N-terminal StrepII-Tag (27) (see Supplementary Table S1). Cells were harvested and disrupted; soluble StCsm complex was captured by Strep-affinity chromatography via tagged Csm2 protein and subjected to size exclusion chromatography.

Cas10 subunit of StCsm complex was expressed and purified as described previously (8). Briefly, pCas10 plasmid was expressed in *E. coli* DH10B (ara$^-$). Cells were harvested and disrupted, Cas10 protein was purified using HisTrap and StrepTrap affinity columns (GE Healthcare).

Full-length WT and mutant StCsm6 and StCsm6′ proteins were expressed and purified as described previously (10). Briefly, *E. coli* DH10B (ara$^-$) was transformed with relevant plasmids (pCsm6, pdCARF-Csm6, pdHEPN-Csm6 or pCsm6′). Cells were grown in LB medium supplemented with an appropriate antibiotic. Cells were harvested and disrupted by sonication, soluble proteins were purified by subsequent His-affinity and Strep-affinity chromatography.

StCsm6 WT and mutant HEPN and CARF domains were expressed in *E. coli* BL21 (DE3) transformed corresponding plasmid (pCARF, pHEPN, pdCARF or pdHEPN). Bacteria were grown at 37°C in LB medium supplemented with ampicillin (50 μg/ml) to the mid-log phase. Expression was induced using 1 mM IPTG and cell suspension was further cultured overnight at 16°C. Cells were harvested and disrupted by sonication, soluble proteins were captured on the HisTrap column (GE Healthcare) using Chromatography buffer (20 mM HEPES (pH 8.0), 0.5 M KCl, 8 mM 2-mercaptoethanol) and 5–500 mM imidazole gradient. Further, to remove the His_{10}-MBP-tag from CARF domain and His_6-tag from HEPN domain, eluted fractions were pooled and incubated with TEV protease (using a 1:50 (w/w) protease:target protein ratio) at 4°C overnight while dialyzing against the Chromatography buffer. Cleaved parts were removed by His-affinity chromatography. Flown-through proteins were dialyzed against 10 mM Tris–HCl (pH 8.0) buffer containing 300 mM KCl, 1 mM DTT, 0.1 mM EDTA and 50% (v/v) glycerol, and stored at −20°C.

Gel filtration analysis of StCsm6 domains

Analytical gel filtration was carried out at room temperature on an ÄKTA FPLC system (GE Healthcare) using a Superdex 75 10/300 GL column (GE Healthcare), pre-equilibrated with the Gel filtration buffer (20 mM HEPES (pH 8.0), 500 mM KCl, 8 mM 2-mercaptoethanol). CARF and HEPN samples at 0.7–0.8 mg/ml loading concentration were prepared in 100 μl of the Gel filtration buffer. Elution from the column was monitored by measuring absorbance at 280 nm. The apparent molecular weights of proteins were evaluated based on the elution volume using a series of standards (Gel filtration Calibration Kit from GE Healthcare).

Plasmid interference assay

Escherichia coli BL21 (DE3) was transformed first with two plasmids encoding the CRISPR–Cas system: (i) the relevant pCRISPR plasmid variant—targeting (pCRISPR_Tc) or non-targeting (pCRISPR_S3) and (ii) WT or mutant plasmid pCas/Csm. Such cells were then grown overnight in liquid LB media supplemented with 2% glucose, streptomycin (25 μg/ml) and chloramphenicol (30 μg/ml), and subsequently transformed with the target pTarget_Tc or control pControl plasmids (see Supplementary Table S1). 1/20 dilutions and non-diluted samples of the transformants were plated on LB media agar plates, supplemented with streptomycin (25 μg/ml), chloramphenicol (30 μg/ml) and ampicillin (50 μg/ml). The cells were grown overnight at 37°C and the resultant colonies were counted. Transformation results of pControl were used to normalize respective results obtained with pTarget_Tc. Arbitrary units of CFU were calculated as CFU(pTarget_Tc)/CFU(pControl).

Bacterial culture preparation for cA_n analysis by HPLC-MS

Escherichia coli BL21 (DE3) cells were first transformed with the two plasmids encoding the CRISPR–Cas system: (i) the relevant pCRISPR variant – targeting (pCRISPR_Tc) or non-targeting (pCRISPR_S3) and (ii) WT or mutant plasmid pCas/Csm. Such cells were subsequently transformed with pTarget_Tc, pTarget_Tc$^{\text{handle mutant}}$ or pControl_Tc plasmids and grown overnight at 37°C in liquid LB media supplemented with 1.5% glucose, streptomycin (25 μg/ml), ampicillin (50 μg/ml), and chloramphenicol (30 μg/ml). Fresh LB medium was inoculated with the overnight culture (1/20 (v/v)) and was further incubated at 37°C. When the culture reached the mid-log phase, expression of the CRISPR–Cas system was induced by addition of 1 mM IPTG. Cell suspension aliquots of 400 ml were taken at indicated time points and pelleted by centrifugation. Before HPLC–MS analysis, biomasses were tested for the presence of the plasmids (at 4 h after induction) by PCR. The presence of intact Cas10 GGDD motif in Palm domain and the Tc-targeting CRISPR region was verified by sequencing the corresponding PCR products.

To demonstrate that different transcript can be used for cA_n synthesis in cells, *E. coli* BL21 (DE3) was transformed first with (i) targeting pCRISPR_GFP or non-targeting pCRISPR_S3 plasmid and (ii) WT or mutant plasmid pCas/Csm. Next, such cells were transformed with the target plasmid pTarget_GFP or pControl_GFP plasmid and grown overnight at 37°C in LB medium supplemented with streptomycin (25 μg/ml), ampicillin (50 μg/ml), chloramphenicol (30 μg/ml) and 1.5% glucose. Fresh LB medium was inoculated with the overnight culture (1/20 (v/v)), and bacteria were grown at 37°C. When they reached the mid-log phase, 1 mM IPTG was added and cells were grown for 4 h before being pelleted by centrifugation.

For phage-induced cA_n assays, pCRISPR_MS2 or pCRISPR_S3 and pCas/Csm_dCsm3_dHDCas10_ΔCsm6′ΔCsm6 plasmids were co-expressed in *E. coli* NovaBlue (DE3), grown at 37°C in LB medium, supplemented with tetracycline (10 μg/ml), streptomycin (25 μg/ml), chloramphenicol (30 μg/ml). Fresh LB medium was inoculated with the overnight culture (1/20 (v/v)), and bacteria were grown at 37°C. When they reached the mid-log phase, 1 mM IPTG was added,

and after additional 30 min the cells were infected by phage suspension. The cells were collected by centrifugation at 16 h post induction.

cA_n detection in bacterial lysates

cA_n-containing fraction was extracted from 100 mg (±5%) bacterial pellet by addition of 2 ml 80% ice-cold methanol prior to sonication, thorough vortexing and centrifugation (16 000 g at 4°C) for 10 min. The supernatants were transferred to new tubes and lyophilized to dryness. The samples were subsequently resuspended in 30 μl solvent A (10 mM ammonium acetate in water, pH 7.0) just before analysis.

2–5 μl of each sample was injected using a Vanquish Horizon UPLC (Thermo Fisher Scientific) or an Agilent 1290 Infinity HPLC system (Agilent Technologies, Santa Clara, CA, USA) equipped with an Agilent Zorbax Eclipse Plus C18 column (2.1 × 150 mm, 1.8 μm) with a 50 mm guard-column, both kept at 40°C. The chromatographic gradient was run at a flow rate of 300 μl/min with the following solvent composition of solvent A and solvent B (acetonitrile): 97% A from 0–2 min, 97–60% A from 2–8 min, 60–10% A from 8–12 min, 10% from 12–15, before equilibration for 3 min with the initial conditions. The flow from the HPLC was coupled to a Q-Exactive HF mass spectrometer (Thermo Fisher Scientific) or Agilent Q-TOF 6530b system (Agilent Technologies) operated in negative ion mode. Data was extracted using Agilent Masshunter Profinder 10.0 or Thermo Xcalibur v. 3.1 with a mass precision of 10 ppm. The cA_ns were annotated based on accurate mass, retention time from synthesized standards and fragment ions. The molar amount of cA_ns was estimated based on comparison to standards of known quantity. The molar concentration of cA_ns was calculated assuming that each *E. coli* cell is 1 fl in volume and its wet weight is 1 pg (30).

In vitro cA_n synthesis assay

The cA_n synthesis reactions were initiated by adding 10 mM $CoCl_2$ or 1 mM $Mg(CH_3COO)_2$ into a mix of 0.2 μM StCsm complex, 0.2 or 10 μM of target RNA S3/1 (27) and 500 μM ATP in the reaction buffer Y (33 mM Tris-acetate (pH 7.6 at 37°C), 66 mM K-acetate, 0.1 mg/ml BSA) or in the Reaction buffer H (20 mM HEPES (pH 7.5), 50 mM KCl, 0.1 mg/ml BSA) and carried out at 37°C for 1 or 16 h. The reactions were stopped by adding 15 mM EDTA. Reaction products were subjected to HPLC-MS analysis.

For time-course experiments, 0.2 μM StCsm complex was mixed with 10 μM target RNA S3/1 (27), 1 mM $Mg(CH_3COO)_2$, 0.5 mM ATP and 10 nM [α-^{32}P]-ATP in the Reaction buffer H. 7 μl aliquots were taken at indicated time points and reactions were quenched by addition of 7 μl 2× RNA loading dye (Thermo Fisher Scientific) supplemented with additional (6.25 mM) EDTA. Radioactively labeled products were analyzed by denaturing PAGE (24% gels, 19:1 acrylamide:bis-acrylamide ratio) and visualized by autoradiography.

α^{32}P-labeled cA_6 for subsequent direct visualization of its hydrolysis products was prepared by mixing 0.2 μM StCsm complex with 10 μM target RNA S3/1 (27), 1 mM $Mg(CH_3COO)_2$, 0.5 mM ATP and 1 μM [α-^{32}P]ATP in the reaction buffer H and incubating at 37°C for ∼16 h. For the control cA_6 hydrolysis reactions with StCsm complex and Cas10 subunit (see Supplementary Figure S4) the synthesized α^{32}P-labeled cA_6 was used without further purification. For all other reactions, synthesis products were separated by denaturing PAGE (24% gels, 19:1 acrylamide:bis-acrylamide ratio) and cA_6 was purified from the gel by phenol extraction and ethanol precipitation.

Synthesis and purification of cA_5

200 nM StCsm was mixed with 200 nM target RNA S3/1 (27) and 17 μM of $pppA_5$ in the Reaction buffer Y and incubated for 20 min at 37°C before initiating the reaction by adding 10 mM $CoCl_2$. The reactions were performed for 1.5 h at 37°C. The reaction products were fractionated by HPLC (Waters Breeze) on the Discovery HS C18 Column (15 cm × 10 mm, 5 μm) (Sigma-Aldrich Supelco) pre-equilibrated with solvent A (100 mM TEAA (pH 7.0)) at room temperature and 1 ml/min flow rate with a linear gradient of B (60% CH_3CN in buffer A) in A (0–100% of B over 100 ml). Fractions containing cA_5 were pooled and the samples were concentrated on a vacuum concentrator (Eppendorf).

In vitro cA_n hydrolysis assay

Unless stated otherwise, cA_n hydrolysis assay was conducted in the Reaction buffer T (40 mM Tris, 20 mM acetic acid (pH8.1 at 25°C), 1 mM EDTA, 0.1 mg/ml BSA) supplemented with 0.5 U/μl RiboLock RNase Inhibitor (Thermo Fisher Scientific) containing 20 μM of synthetic cA_6 (Biolog), synthetic cA_4 (Biolog), linear A_6>p (ChemGenes) or ∼30 μM of StCsm-produced cA_ns mixture. Reactions were started by adding an indicated amount (0–10 μM) of protein and incubated at 37°C. Reactions were stopped by freezing and subjected to HPLC-MS analysis.

To directly visualize the hydrolysis of cA_6, reactions were conducted in the Reaction buffer T supplemented with 0.5 U/μl RiboLock RNase Inhibitor (Thermo Fisher Scientific) and contained 50 nM of StCsm-produced radioactively labeled α^{32}P-cA_6. Multiple turnover reactions contained additionally 10 μM of unlabeled cA_6 (Biolog). Reactions were started by adding an indicated amount (0–10 μM) of protein and were carried out at 37°C. 5 μl aliquots were taken at indicated time points and reactions were quenched by mixing with equal amount of 2× RNA Loading Dye (Thermo Fisher Scientific). Reaction products were analysed by denaturing PAGE (24% gels, 19:1 acrylamide:bis-acrylamide ratio) and visualized by autoradiography. For single turnover reactions, k_{obs} were determined by fitting a single exponential to the substrate depletion data. For k_{cat} calculation, the reaction rates were determined from the linear parts of the reaction progress curves by linear regression.

For the control cA_6 hydrolysis reactions (presented in Supplementary Figure S4), 10 μM of α^{32}P-labelled cA_6 was taken from the synthesis mixture and incubated with 10 μM of unlabeled cA_6 (Biolog), 10 nM of protein (StCsm or Cas10) in the Reaction buffer Y in the absence or presence of target RNA S3/1 (27) and 10 mM of Mg^{2+}, Mn^{2+},

Co^{2+} or Ni^{2+} at 37°C for 8.5 h. Reaction products were separated by denaturing PAGE (24% gels, 19:1 acrylamide:bis-acrylamide ratio) and visualized by autoradiography.

In vitro RNA hydrolysis assay

RNA hydrolysis reactions were conducted in the reaction buffer T, supplemented with 0.5 U/μl RiboLock RNase Inhibitor (Thermo Fisher Scientific) and additional 1 mM EDTA. Reactions contained 10 nM of 5′-^{32}P-radiolabeled RNA NS (27) and 0–1 μM cA_6 (Biolog) or 0–100 nM cA_5 synthesized from the $pppA_5$ precursor. Reactions were started by adding 0–10 μM StCsm6 or its isolated domains and were carried out at 37°C. The reaction products were separated by denaturing PAGE (15% gels, 29:1 acrylamide:bis-acrylamide ratio) and visualized by autoradiography.

Electrophoretic mobility shift assay

0.2 nM of 5′-^{32}P-radiolabeled RNA NS (27) was incubated with different amounts (0–3 μM) of CARF domain or (0–1 μM) of dHEPN domain in the Reaction buffer T for 10 min at room temperature. Reaction mixtures were analyzed by native PAGE and visualized by autoradiography.

RNA hydrolysis competition assay

RNA hydrolysis reactions were performed at 25°C and contained 10 nM of 5′-^{32}P-radiolabeled RNA NS (27) and 0–500 μM of cA_6 in reaction buffer Y. Reactions were initiated by addition of StCsm6 to the final concentration of 10 nM. 5 μl aliquots of the samples were collected at indicated time intervals and quenched by mixing with 2× RNA loading dye (Thermo Fisher Scientific). The reaction products were separated by denaturing PAGE (15%, 29:1 acrylamide:bis-acrylamide ratio) and visualized by autoradiography**.** RNA hydrolysis constants k_{obs} were determined by fitting a single exponential to the substrate depletion data.

HPLC-MS analysis of Csm6 cA_n hydrolysis products

To analyze the cA_n hydrolysis products, electrospray ionization mass spectrometry (ESI-MS) was performed in negative mode using an integrated HPLC/ESI-MS system (1290 Infinity, Agilent Technologies/Q-TOF 6520, Agilent Technologies) equipped with a Supelco Discovery® HS C18 column (7.5 cm × 2.1 mm, 3 μm). Elution was performed with a linear gradient of solvents A (5 mM ammonium acetate in water, pH 7.0) and B (5 mM ammonium acetate in methanol, pH 7.0) at a flow rate of 0.3 ml/min at 30°C as follows: 0–2 min, 0% B; 2–22 min, 20% B; 22–25 min, 50% B, 25–29 min 100% B. Ionization capillary voltage was set to 5000 V, fragmentor—to 150V. The cA_n hydrolysis products were annotated based on accurate mass, retention time from synthesized standards and fragment ions.

Treatment of StCsm6 cA_6 hydrolysis products with P1 nuclease

11 μl of the StCsm6 cA_6 hydrolysis reaction or 20 μM of control compound (A_6>p or A_3) was incubated with 10 mU P1 nuclease (Sigma) in the P1 Reaction buffer (10 mM Tris-acetate (pH 7.1 at 37°C), 1 mM Zn-acetate) at 37°C for 1 h. Reaction was stopped by adding 5mM EDTA to the reaction mixture and heating at 75°C for 10 min. 10 μl of this reaction mix was diluted with water and subsequently subjected to HPLC-MS analysis.

5′-Labeling of StCsm6 cA_6 hydrolysis products

11 μl of StCsm6 cA_6 hydrolysis reaction or 20 μM of control compound (A_2 or A_3) was incubated with 1 U T4 polynucleotide kinase (PNK) and 500 μM ATP in the reaction buffer PNK A (50 mM Tris–HCl (pH 7.6 at 25°C), 10 mM $MgCl_2$, 5 mM DTT, 1 mM spermidine) at 37°C for 30 min. Reaction was stopped by adding EDTA to the final concentration of 5 mM and heating at 75°C for 10 min. Such reaction mixture was subsequently subjected to HPLC-MS analysis.

Prediction of the StCsm6 CARF active site

Blastp (31) was used to find StCsm6-CARF domain homologs with 20–28% sequence identity (maximum target sequences 20,000). Multiple alignment was performed with MultAlin (32) and the figure was prepared with ESPript 3.0 (33).

topp (34) was used to superpose StCsm6-CARF domain model (10) and ToCsm6-cA_4 structure (25). Figure of StCsm6 CARF-cA_4 model was prepared using PyMOL (35).

Quantification and statistical analysis

Data analysis was performed using Kyplot 2.0 software (36). Determined cA_6 hydrolysis rate constants are presented as the optimal value ±1 standard deviation.

RESULTS

Plasmid interference by *S. thermophilus* type III-A CRISPR–Cas system in the heterologous *E. coli* host

We repurposed the *S. thermophilus* Type III-A CRISPR–Cas system expressed in heterologous *E. coli* strain (27) to investigate CRISPR immunity *in vivo* using plasmid interference assay (Figure 1A). In brief, *E. coli* host contained two recombinant plasmids: pCas/Csm plasmid expressing all Cas/Csm proteins, except for *cas1* and *cas2*, and pCRISPR_Tc plasmid carrying a CRISPR array containing 4 copies of spacer targeting the transcript of tetracycline resistance gene (Tc^R) gene. We transformed these cells with pTarget_Tc plasmid and plated transformants with respective antibiotic combinations (Figure 1B). As a control, we used *E. coli* cells containing the pCas/Csm plasmid and a pCRISPR_S3 plasmid that carried 4 copies of non-targeting S3 spacer (Supplementary Table S1). In the presence of WT StCsm complex, transformation of pTarget_Tc plasmid into *E. coli* expressing Tc-targeting crRNA resulted in ∼100-fold fewer transformants, as compared to the non-targeting S3 crRNA expressing cells (Figure 1C). This shows that StCsm-mediated immunity is manifested in the heterologous *E. coli* host and it depends on target transcription as

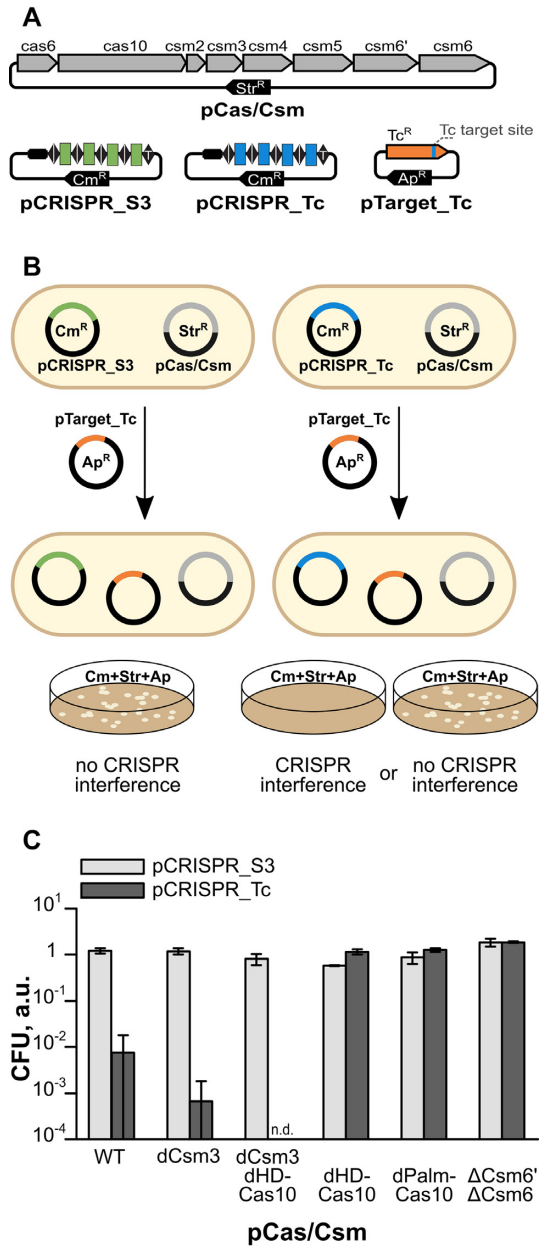

Figure 1. Plasmid interference by *S. thermophilus* type III-A CRISPR–Cas system in heterologous *E. coli* host. (**A**) Plasmids used in this study. See Supplementary Table S1 for more information. (**B**) Plasmid interference assay. *E. coli* expressing Tc^R transcript-targeting and non-targeting StCsm complexes (WT or mutant) were transformed with the target plasmid and plated with respective antibiotics. (**C**) Arbitrary number of colony forming units (CFU) of *E. coli* expressing targeting StCsm complex (dark grey) or non-targeting StCsm complex (light gray) are plotted for at least two replicates. CFU were calculated as described in Materials and Methods. Error bars indicate standard deviation between the replicates. n.d. – not detected.

it was suggested by *in vitro* experiments (8). Notably, even though both *cas*/*csm* genes and CRISPR array were under an IPTG-inducible promoter, the plasmid interference manifested in the absence of IPTG, indicating that traces of the StCsm complex produced due to the promoter leakage are sufficient to provide immunity against exogenic DNA.

To establish the role of different enzymatic activities in plasmid immunity, the interference assay was conducted with pCas/Csm variants (Supplementary Table S1) that carried inactivating mutations: D33A in the Csm3 RNase subunit (dCsm3), D575A and D576A in the Cas10 Palm domain (dPalm-Cas10), D16A in Cas10 HD-nuclease domain (dHD-Cas10), or both StCsm6′ and StCsm6 deletion variants (ΔCsm6′ΔCsm6). In the case of dCsm3, the transformation efficiency was ∼10-fold lower in comparison to the WT StCsm (Figure 1C) suggesting that the Csm3-dependent RNase activity is not required for immunity and might even down-regulate it by constantly cutting the target RNA, required for Cas10 activation. Meanwhile disruption of any other enzymatic activity levelled target plasmid transformation efficiency to that of non-targeting plasmid (Figure 1C) suggesting that both DNA degradation and cA_n signaling pathways are required for *S. thermophilus* type III-A CRISPR–Cas mediated immunity. Intriguingly, simultaneous inactivation of both Csm3 RNase and Cas10 DNase secured efficient plasmid interference, implying that in the absence of Csm3 RNase activity, the cA_n-dependent pathway alone is able to provide plasmid immunity, as Csm3 inactivation results in a constant and a high production of cA_n (10,12).

Monitoring cA_n production *in vivo*

We have previously shown that StCsm complex *in vitro* synthesizes cA_ns (n = 2–6) from ATP. cA_3 was identified as the major reaction product; however, only the minor cA_6 product activated StCsm6 RNase (10). To get an insight into StCsm6 RNase activation mechanisms in the cell, we decided to examine cA_n metabolites produced *in vivo* in the heterologous *E. coli* host expressing the *S. thermophilus* type III-A CRISPR–Cas system. To monitor amount of the cyclic adenylates produced in *E. coli* we employed high-performance liquid chromatography-mass spectrometry (HPLC-MS) technique. In these experiments we used the same *E. coli* host as in the interference assay (Figure 1A), except that the inducer IPTG was added to the cell culture. To prevent RNA and DNA degradation by the CRISPR–Cas system and ensure cell viability, we used a pCas/Csm variant where all proteins' activities except that of the Cas10 Palm synthase have been inactivated by mutations (dCsm3, dHD-Cas10, ΔCsm6′ΔCsm6) (Supplementary Table S1). Such setup enabled monitoring of cA_n level in the host constitutively expressing the targeted Tc^R gene in the pTarget_Tc plasmid. Targeted HPLC-MS analysis reported various cA_ns, from $n = 2$ up to 6 but the equilibrium was significantly shifted towards cA_5 and cA_6 species (Figure 2A and Supplementary Figure S1A). The cA_5 and cA_6 amount was significantly increased during the first 4 h after IPTG induction to 22.3 ± 4.6 and 12.9 ± 3.8 pmol/mg of wet cell culture, which translates to 22.3 ± 4.6 and 12.9 ± 3.8 μM concentration in the *E. coli* cell. The amount of cA_5 and cA_6 detected in the heterologous *E. coli* host is comparable to the amount of the c-di-AMP metabolite (13.8 ± 1.1 pmol/mg) present in the *Streptococcus suis* host (37). Interestingly, after 8 hours post-induction, the amount of cA_5 and cA_6 had slightly decreased while cA_3 and cA_4 kept increasing (Figure 2A). It cannot be excluded that in

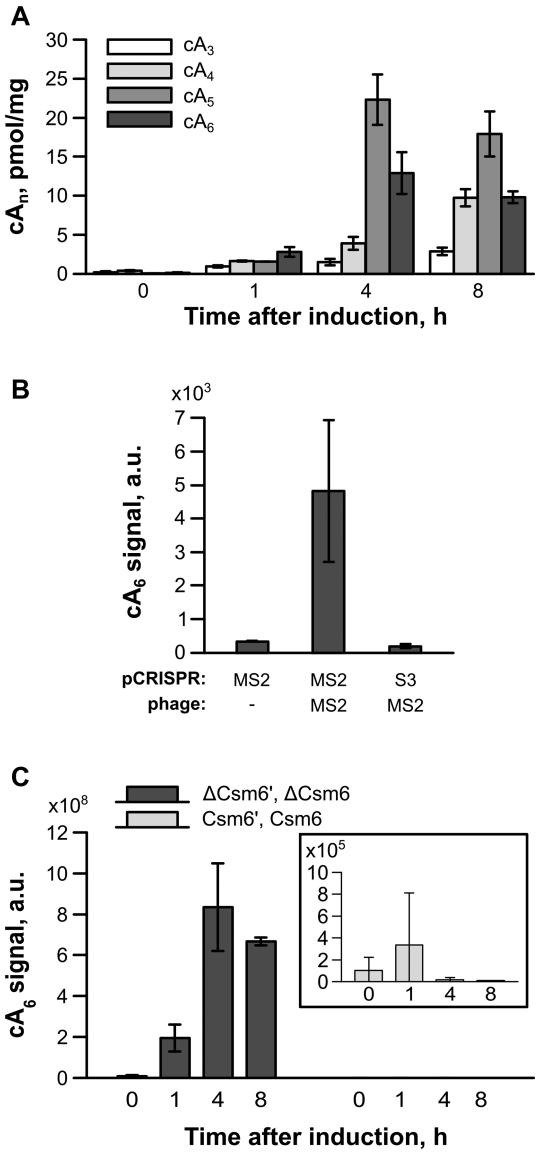

Figure 2. cA_n synthesis by StCsm complex *in vivo* analyzed by HPLC-MS. (**A**) *E. coli* harboring plasmids (as indicated in Figure 1A and Supplementary Table S1) encoding the Tc^R transcript and expressing StCsm complex mutant (dCsm3, dHD-Cas10 and ΔCsm6′ΔCsm6) targeting Tc^R were grown in the presence of inducer IPTG. The samples were taken at defined time points after induction and cA_n amount was analyzed by HPLC-MS. (**B**) Analysis of cA_6 produced in *E. coli* cells, which express StCsm complex mutant (dCsm3, dHD-Cas10 and ΔCsm6′ΔCsm6) targeting MS2 transcripts, after 16 h of phage MS2 infection. (**C**) HPLC-MS analysis of cA_6 amount changes over time *in vivo* in the absence (left) or presence (right) of StCsm6 and StCsm6′ encoding genes. The inset depicts the same data on a different scale.

this case the decrease in total cellular ATP concentration shifts the ATP polymerization:cyclisation reaction equilibrium to shorter reaction products.

We have previously shown that for *in vitro* cA_n synthesis the following conditions must be met: (i) spacer sequence of crRNA must be complementary to the protospacer sequence of target RNA, (ii) the 3′-flanking sequence of the target RNA must not base-pair with the 5′-handle of crRNA and (iii) Cas10 in the effector complex must contain an intact GGDD-active site in the Palm domain (10). HPLC-MS analysis of cA_6 metabolites in *E. coli* (Supplementary Figure S2A) confirmed the cA_n synthesis requirements established *in vitro* for *S. thermophilus* and other type III systems (10,11,13–15).

To probe whether cA_6 is produced in response to phage infection, we performed HPLC-MS analysis of cA_n metabolites in the phage-infected cells. Heterologous *E. coli* host carrying pCas/Csm and pCRISPR_MS2 plasmids (Supplementary Table S1) was infected with RNA coliphage MS2 (27). Targeted HPLC-MS analysis revealed accumulation of cA_5 and cA_6 in response to MS2 phage infection (Figure 2B and Supplementary Figure S1B). Taken together, analysis of cA_n metabolites in *E. coli* cells demonstrates that the type III-A CRISPR–Cas system in the heterologous host produces signaling molecules in response to exogenic nucleic acids that derive either from plasmid or phage.

Optimization of cA_6 synthesis *in vitro*

HPLC-MS analysis of cA_ns produced in *E. coli* cells revealed an altered cA_n profile in comparison to *in vitro* experiments (10), suggesting that discrepancies in the size distribution could arise due to different reaction conditions. Therefore, we re-evaluated cA_6 synthesis *in vitro* using a different StCsm: target RNA ratios, buffers and Co^{2+} or Mg^{2+} ions as cofactors (Supplementary Figure S3A). We found a significant shift in the cA_n size distribution profile towards a larger ring size and ultimately to cA_6 in the presence of target RNA excess and Mg^{2+}. Interestingly, prolonged incubation of StCsm with ATP resulted in a slightly increased cA_3 and cA_4 yield *in vitro* (Supplementary Figure S3A, lane x), in line with *in vivo* HPLC-MS data (Figure 2A, 8 h point), even though Csm3 D33A mutation abolishes target RNA cleavage.

cA_n profile *in vivo* in the presence of StCsm6

The cA_n-dependent RNA-degradation pathway has to be switched-off once the exogenic nucleic acid is eliminated, raising the question of how cyclic oligoadenylate concentration is regulated in the cell. HD domain phosphodiesterases, that are widespread in bacteria, are often involved in cA_2 degradation in the cell (38). While the Cas10 subunit of StCsm contains an HD domain, which is involved in ssDNA degradation (8), we did not detect any cA_n degradation by either isolated Cas10 or the StCsm complex (Supplementary Figure S4A). It has been recently shown that some CARF domain-containing proteins act as ring nucleases that degrade cA_4 molecules (22–25). We reasoned that the CARF domain of StCsm6 could also degrade the cA_6 activator. Analysis of cA_6 amount in the cell provided indirect support for this hypothesis: *E. coli* cells expressing WT StCsm6′ and StCsm6 exhibited drastically reduced levels of cA_6 and other cA_n (Figure 2C and Supplementary Figure S1C) suggesting that StCsm6 proteins are responsible for cA_n degradation in the cells.

StCsm6 cleaves cA_6 *in vitro*

To investigate whether Csm6 proteins degrade cA_ns, we isolated individual StCsm6 and StCsm6′ proteins and studied their activities *in vitro*. In the absence of divalent metal ions both proteins degraded radiolabeled cA_6, generating faster migrating products in denaturing PAGE (Figure 3B and Supplementary Figure S4B). HPLC-MS analysis revealed a mixture of three cleavage products, namely cAMP (2′,3′-cyclic AMP (A>p) or 3′,5′-cyclic AMP), and linear or cyclic di- and tri-adenylates (Figure 3B and Supplementary Figure S4B). To differentiate between cyclic (cA_n) and terminal 2′,3′-cyclic phosphate-containing linear oligoadenylates (A_n>p), we further treated these products with P1 nuclease and polynucleotide kinase (PNK). Subsequent HPLC-MS analysis confirmed that StCsm6 reaction products are converted to adenosine and AMP by P1 nuclease, suggesting an asymmetric structure of the substrate. Moreover, these products could be 5′-labeled by PNK to produce di- and tri-adenylate phosphates, confirming the presence of a free terminal 5′-OH group (Supplementary Figure S5). Together these experiments are consistent with a linear structure of the products, suggesting that StCsm6 in the absence of metal ions degrades cA_6 into a mixture of A>p, A_2>p and A_3>p. This is not surprising, since cyclic-2′,3′ phosphate products are usually generated by other metal-independent RNases like ribonuclease A, Cas6 and tRNA splicing endonuclease (39,40).

cA_6 degradation by isolated CARF and HEPN domains

According to HPLC-MS analysis, *E. coli* cells in the presence of StCsm6 and StCsm6′ RNases exhibit drastically reduced levels of cA_6 and other cA_ns (Figure 2C and Supplementary Figure S1C), suggesting their involvement in cA_n degradation. StCsm6 is comprised of CARF and HEPN domains. It has been previously shown that the CARF domain of other, cA_4-dependent, Csm6 proteins is able to cleave the cA_4 activator (24,25), implying a similar function for the StCsm6 CARF domain. On the other hand, the HEPN domain of StCsm6 protein is a RNase, which digests RNA even in the absence of the cA_6 activator albeit at high concentrations (10); therefore, it is possible that it could also degrade cA_6. To establish which domain is responsible for cA_6 cleavage, we engineered and purified individual CARF (1–169 aa) and HEPN (172–428 aa) domains of StCsm6 (Figure 3A and Supplementary Figure S6A) that both remained dimers in solution (Supplementary Figure S6B) like WT StCsm6 (10). Isolated HEPN domain degraded linear RNA at the same rate as WT StCsm6 in the absence of activator (Supplementary Figure S7).

Next, we analyzed cA_6 degradation activity of individual CARF and HEPN domains. Surprisingly, both CARF and HEPN domains were able to degrade radiolabeled cA_6; however, under single turnover conditions the CARF domain was much more efficient at degrading cA_6 than the HEPN domain (Figures 3C and D). Mutations of HEPN active site residues R371A and H376A (10) required for RNase activity dramatically impaired hydrolysis of both cA_6 (Figure 3D) and linear RNA (Supplementary Figure S7C), indicating that the same active site is responsible for cA_6 and linear RNA cleavage.

To predict the putative active site of CARF in StCsm6, we superposed StCsm6 CARF domain model (10) with *T. onnurineus* Csm6-cA_4 structure (PDB ID: 6O6V) (25) and identified that conserved D12, S105 and T107 residues of StCsm6 are located near the cyclic oligoadenylate (Supplementary Figure S8). While S105 and T107 are important for cA_6 binding (10), D12A mutation (dCARF variant) completely abolished the cA_6 hydrolysis activity of the CARF domain (Figure 3C), indicating that this residue is important for cA_6 cleavage.

Next, we analyzed reaction products generated by CARF and HEPN domain-mediated cleavage of cA_6. HPLC-MS analysis revealed that the CARF domain converts cA_6 to A_3>p; however, linear A_6>p is also present in the reaction mixture (Figure 3C) and can be further cleaved by CARF into the final reaction product, A_3>p (Supplementary Figure S7D). Presumably, each monomer of homodimeric CARF domain cuts cA_6 producing A_3>p, similarly to the ring nucleases that split cA_4 into two A_2>p (22). The reaction occurs non-concertedly since A_6>p product is identified in the reaction mixture. Unlike CARF domain, HEPN domain degraded cA_6 into a mixture of A_6>p, A_4>p, A_3>p, A_2>p and A>p oligoadenylates (Figure 3D). Together, this shows that both StCsm6 domains function as metal-independent ring nucleases that degrade cA_6 but generate different cleavage products.

cA_6 degradation by the full-length StCsm6

We found that isolated CARF and HEPN domains of StCsm6 both are capable of degrading cA_6; moreover, binding of cA_6 to the CARF domain allosterically stimulates RNase activity of the HEPN domain (10). Therefore, we next examined possible allosteric connection between the CARF and HEPN domains in cA_6 degradation by the WT StCsm6. To dissect possible allosteric interactions between the domains, we compared cA_6 cleavage by WT StCsm6 and mutants that were deficient in cA_6 cleavage in either CARF (dCARF-Csm6) or HEPN (dHEPN-Csm6) domains (Figure 3E).

Under enzyme excess (E>>S) conditions, dHEPN-Csm6 cleaved cA_6 at the rate ($k_{obs(dHEPN\text{-}Csm6)} = 0.27 \pm 0.10$ min^{-1}) that was comparable to the WT StCsm6 ($k_{obs(WT)} = 0.19 \pm 0.04$ min^{-1}) and about 2-fold slower than the isolated CARF domain ($k_{obs(CARF)} = 0.47 \pm 0.18$ min^{-1}) (Figures 3B, C and E). This suggests that at low cA_6 concentrations CARF domain of StCsm6 functions as a ring nuclease, and the contribution of HEPN domain is negligible. Indeed, dCARF-Csm6 variant cleaved cA_6 very slowly, similarly to the isolated HEPN domain (Figures 3D and E).

Low cA_6 degradation activity of the HEPN domain (Figure 3D) may be due to poor binding of cA_6. We were unable to determine cA_6 binding affinity of the HEPN domain directly; therefore, we indirectly evaluated cA_6 binding using a cleavage competition assay. We mixed full-length WT StCsm6 and RNA at a 1:1 ratio, and measured the cleavage rate of RNA in the presence of increasing concentrations of cA_6 (Figure 4A). At low cA_6 concentrations StCsm6 hydrolyzed RNA very slowly because HEPN was not allosterically activated by cA_6 binding in the CARF domain. RNA hydrolysis rate increased significantly at 10 nM of cA_6, im-

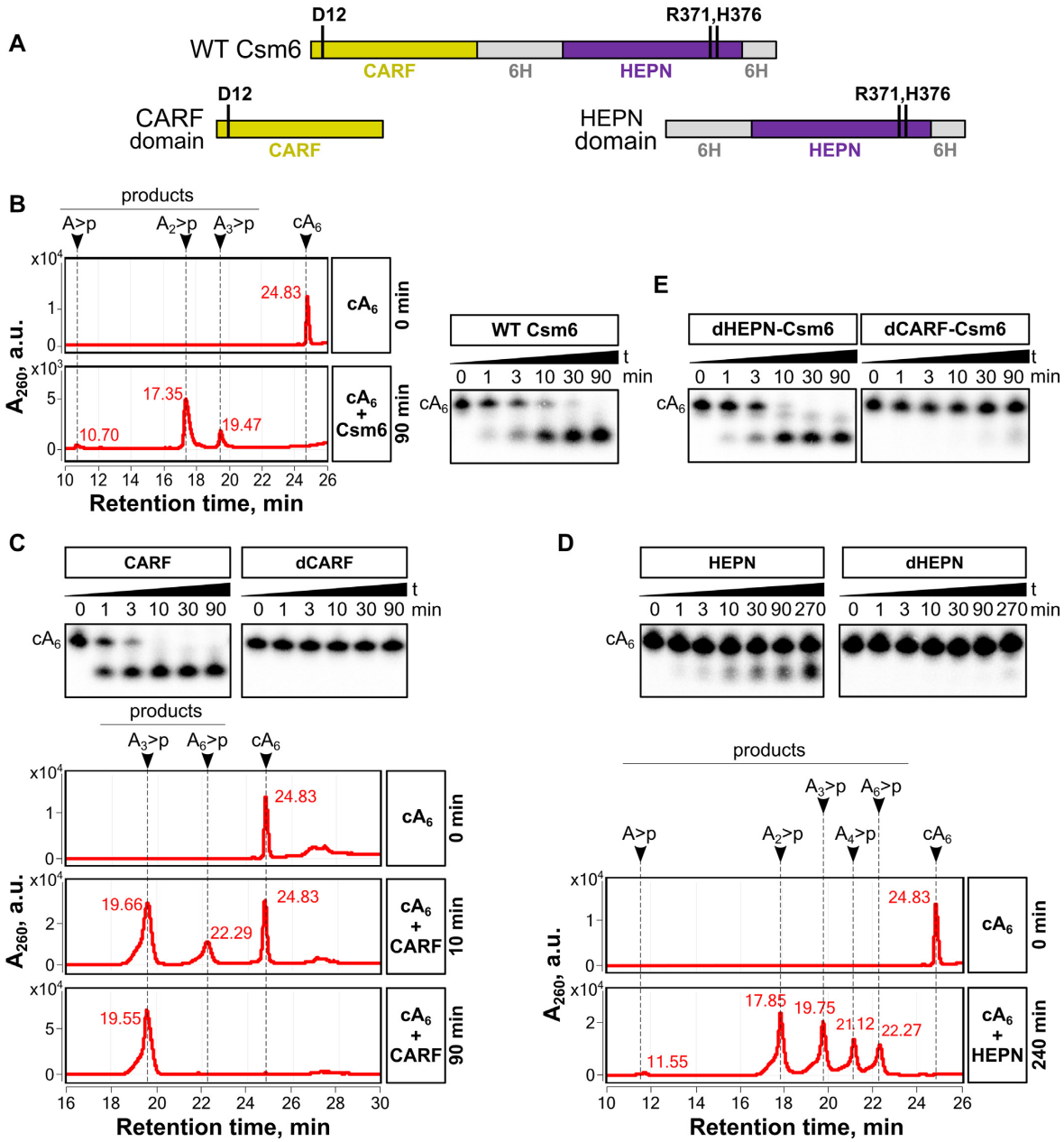

Figure 3. cA_6 hydrolysis by CARF and HEPN domains of StCsm6 *in vitro*. (**A**) Schematic illustration of WT StCsm6 protein and its CARF (1–169 aa) and HEPN (172–428 aa) domains. Residues important for activity are indicated. *In vitro* hydrolysis of cA_6 by (**B**) WT StCsm6, (**C**) isolated CARF domain, (**D**) isolated HEPN domain and (**E**) full-length StCsm6 with R371A, H376A (dHEPN-Csm6) and D12A (dCARF-Csm6) mutations, as analyzed by PAGE and HPLC-MS. All cA_6 hydrolysis reactions analyzed by PAGE contained 50 nM of α^{32}P-labeled cA_6 and 1 μM of WT, CARF, dHEPN-Csm6 or dCARF-Csm6, or 10 μM of HEPN. MS reactions contained 20 μM of non-labeled cA_6 and 10nM of WT, 1 μM of CARF or 10 μM of HEPN.

plying cA_6 binding in the CARF domain and allosteric activation of the RNase activity of HEPN domain. Further increase of cA_6 concentration up to 100 nM did not change RNA hydrolysis rate. Inhibition of RNA hydrolysis was observed at cA_6 concentrations above 100 μM (Figure 4A), suggesting that HEPN has lower binding affinity towards cA_6 than CARF domain.

Therefore, we next analyzed StCsm6 cA_6 cleavage under multiple turnover (S>E) conditions. Under these conditions WT StCsm6 rapidly degraded cA_6 with a turnover rate of >20 min^{-1} (Figure 4B). It is likely that at high concentrations cA_6 binds both to CARF and HEPN, thereby allosterically activating effective degradation of cA_6 by the HEPN nuclease. In contrast, isolated CARF domain and HEPN-deficient dHEPN-Csm6 cleaved cA_6 significantly slower (k_{cat} <0.1 min^{-1}). Taken together, these results suggest that an activated HEPN is a much more efficient ring nuclease than CARF. The dCARF-Csm6 mutant with impaired cA_6 cleavage at the CARF domain degraded cA_6 much faster than isolated HEPN domain (Figure 4B), indicating that cA_6 binding but not cleavage is required for activation of the HEPN ring nuclease. The slower cA_6 cleavage

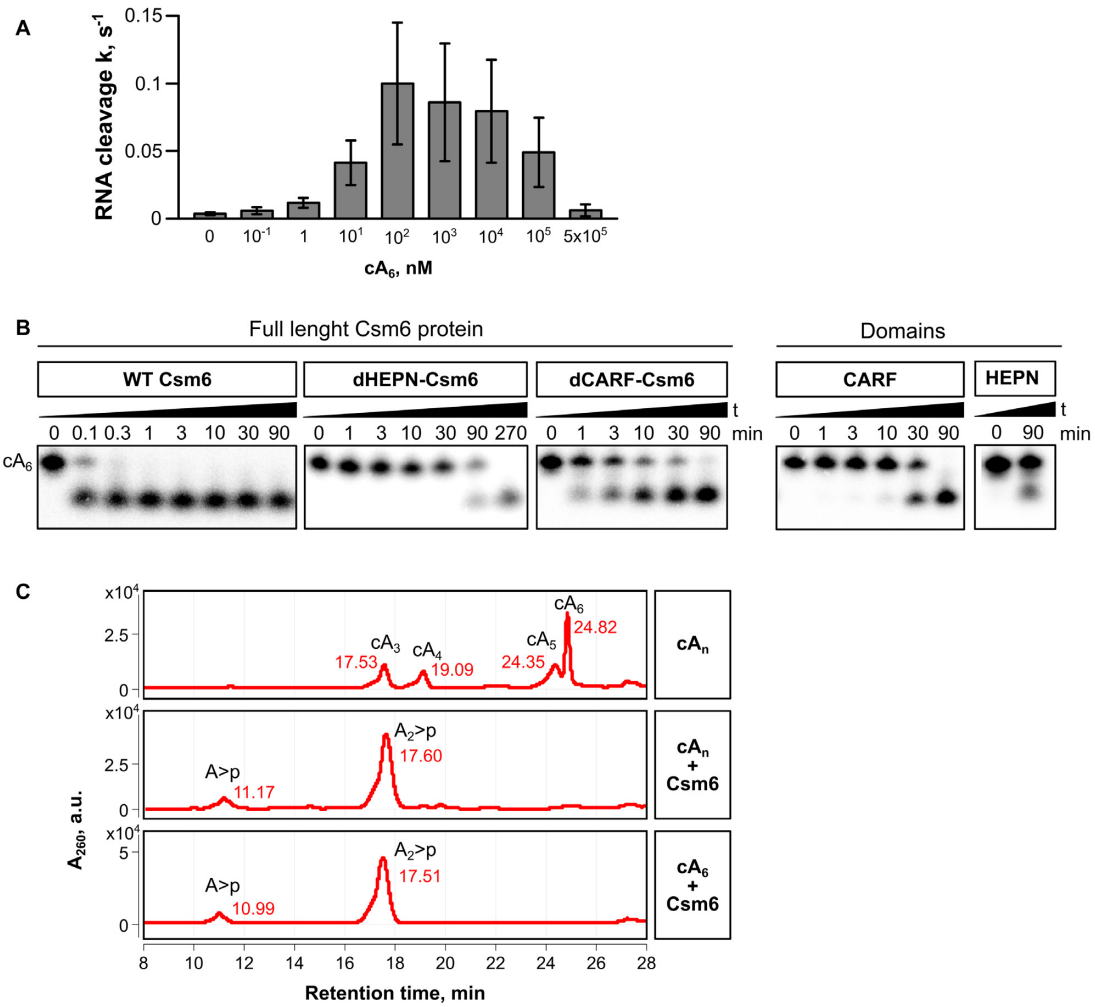

Figure 4. cA_6 hydrolysis by the HEPN domain of StCsm6 *in vitro*. (**A**) RNA hydrolysis competition assay. RNA hydrolysis rate of WT StCsm6 (10 nM ^{32}P-labeled RNA, 10 nM StCsm6) was monitored in the presence of increasing concentration (0–500 μM) of cA_6. (**B**) cA_6 hydrolysis under multiple turnover conditions. 1 μM of full-length WT StCsm6 or its CARF and HEPN mutant variants were mixed with 50 nM α^{32}P-labeled cA_6 and 10 μM of non-labeled cA_6 and its hydrolysis products were analyzed by PAGE. (**C**) cA_n hydrolysis by WT StCsm6. A mixture of cA_ns (~30 μM) produced by the StCsm complex was incubated with 10 nM WT StCsm6 for 90 min and analyzed by HPLC-MS.

by the dCARF-Csm6 mutant as compared to WT may result from compromised cA_6 binding affinity, caused by the D12A mutation in the CARF domain. In agreement with impaired cA_6 binding, an increased cA_6 concentration (up to 300 nM) was required for activation of RNA degradation by the dCARF-Csm6 mutant (Supplementary Figure S7E).

cA_n degradation by StCsm6

HPLC-MS analysis revealed that in *E. coli* host expressing StCsm6 and StCsm6′ RNases, the level of all cA_ns is dramatically decreased (Figure 2C and Supplementary Figure S1C), suggesting that StCsm6 is capable of degrading different cA_ns including cA_6 produced by the Csm effector complex. We found that after prolonged incubation StCsm6 converted a mixture of cA_ns to A_2>p and A>p (Figure 4C). Isolated CARF domain failed to cleave cA_3 and cA_4 in the mixture of cA_n but was able to convert cA_6 to A_3>p and linearize cA_5 (Supplementary Figure S9A). However, cA_5-bound CARF did not activate RNase activity of the HEPN domain of WT StCsm6 (Supplementary Figure S9B). Isolated HEPN domain was not as effective in converting cA_ns to A_2>p as the full-length StCsm6 (Figure 4C and Supplementary Figure S9A).

Together, these results show that StCsm6 has two ring nuclease activities: the CARF domain, which is specific to cA_6 and upon cleavage produces A_3>p, and the HEPN domain, which upon allosteric activation indiscriminately degrades cA_n (n = 3–6) oligoadenylates down to A>p.

DISCUSSION

Type III CRISPR–Cas systems are complex, versatile and efficient barriers protecting host cells against foreign nucleic acids (41). We have previously shown that in the *S. thermophilus* type III-A CRISPR–Cas system, target RNA binding by the StCsm effector complex activates the Cas10 protein, whose HD domain starts ssDNA degradation, and the Palm domain initiates synthesis of cyclic cA_ns (n = 2–6) (8,10). The cA_6 produced in response to viral infection acts

as a signaling molecule that binds to the CARF domain of the stand-alone StCsm6 and StCsm6′ proteins and allosterically activates the non-specific ribonucleolytic activity of their HEPN domains (10). Here, we aimed to establish the control and regulation mechanisms of the cA_6-dependent StCsm6 RNase both *in vitro* and *in vivo*.

cA_5 and cA_6 are major reaction products produced in the cell

While the target plasmid degradation by the Cas10 DNase has been monitored in cells over time (3,20), the Cas10-mediated cA_n synthesis in cells has not yet been analyzed. Using targeted HPLC-MS analysis we show that in response to the target sequence transcription from a plasmid or a phage, *S. thermophilus* type III-A CRISPR–Cas system in heterologous *E. coli* host produces cA_ns of different ring size (Figure 2). The cyclic oligoadenylates with larger ring sizes ($n = 5$–6) were most abundant, including cA_6, that binds to the sensor CARF domain and activates StCsm6 and StCsm6′ RNases. The cA_n size distribution detected in the cell matched that observed *in vitro* under high target RNA concentrations (Supplementary Figure S3). In addition to cA_5 and cA_6, significant amount of cA_4 and cA_3 was also detected (Figure 2A). Bacterial cGAS/DncV-like nucleotidyltransferases synthesize cyclic tri-nucleotide compounds (42) including cA_3 that activate restriction enzyme-like endonuclease effector NucC in the bacteriophage immunity pathway (43,44). It cannot be excluded that cA_3 produced by the type III systems could contribute to alternative pathways in bacterial signaling, such as NucC activation.

Self-regulation of the cA_n signaling pathway

Plasmid interference experiments revealed (Figure 1C) that, in agreement with previous type III studies (12,20,45,46), both ssDNA degradation and cA_n signaling pathway are required for *S. thermophilus* type III-A CRISPR–Cas mediated immunity. Notably, *E. coli* cells do not survive when they carry heterologous type III CRISPR–Cas system with catalytically deficient Csm3 and DNase variants (Figure 1C), indicating that cA_6-activated StCsm6 and StCsm6′ RNases alone enable plasmid immunity. Since cA_n signaling pathway is critical for CRISPR–Cas type III immunity, it must be regulated to avoid host damage. First, cA_n synthesis should be switched-off once the foreign transcript is eliminated, and next, cA_n messengers produced in response to infection should be cleared from the cell. Csm3 RNase controls cA_n level at the synthesis stage through degradation of target RNA that is required for initiation of cA_n synthesis (10,14). Csm3 inactivation results in higher cA_n production yield *in vitro* (10,12). In the cell, it should promote upsurge in cA_n production and subsequent increase of StCsm6 RNase activity, which may cause dormancy (47,48) or cell death. Uncontrollably enhanced StCsm6 RNase activity presumably ensures plasmid immunity in the case of DNase-deficient variant of StCsm (Figure 1C).

HPLC-MS analysis of cell metabolites revealed that in the presence of StCsm6 and StCsm6′, cA_ns, including cA_6, are depleted from *E. coli* cells (Figure 2C and Supplementary Figure S1C). CARF ring nucleases were recently shown to be responsible for degradation of specific cA_4 messengers (22–25). However, in the *S. thermophilus* type III-A system cA_ns are degraded by StCsm6 independently of the ring size, suggesting a different cA_n degradation pathway. Indeed, we show here that both CARF and HEPN domains of StCsm6 proteins function as ring nucleases but exhibit different binding specificities and produce distinct reaction products (Figures 3 and 4).

StCsm6 CARF is a cA_6-specific ring nuclease

Isolated StCsm6 CARF ring nuclease shows no activity either on linear RNA or cA_4 (Supplementary Figures S7B and S9A) but tightly binds cA_6 and converts it to A_3>p (Figures 3C and 4A). Similarly to other CARF ring nucleases (22,24) cleavage of cA_6 by StCsm6 CARF domain is slow (Figures 3 and 4). Identification of the linear A_6>p intermediate during the reaction (Figure 3D) suggests that both active sites in CARF dimer act independently. Similarly, it has been reported that *T. onnurineus* Csm6 CARF domain cleaves cA_4 first to produce A_4>p and subsequently to A_2>p (25). CARF is also able to bind and linearize cA_5 (Supplementary Figure S9A). However, cA_5 is not an optimal substrate for the CARF ring nuclease and is only cleaved by one of the active sites of the CARF domain dimer.

Aspartate D12 is proposed as a catalytic residue in the StCsm6 CARF domain since D12A mutation abolishes cA_6 cleavage activity (Figure 3C). Catalytic residues identified in ring nucleases are very diverse: D12 in Csm6 of *S. thermophilus*, T10/T11 in Csm6 of *T. thermophilus*, W14 in Csm6 of *T. onnurineus* and Y14 in Csx1 of *S. islandicus* (23–25). Variation of catalytic residues in the active sites of CARF domains argues that there are multiple ways for positioning and activation of 2'-OH group of the ribose for nucleophilic attack that results in the phosphodiester bond cleavage during cyclic oligoadenylate (cA_4 and cA_6) degradation. Recent structural and biochemical study of *Enterococcus italicus* Csm6, published during preparation of this manuscript, also revealed that CARF domain is capable of cleaving cA_6 (49).

cA_6-binding at CARF domain promotes HEPN-mediated degradation of RNA and cA_ns

In contrast to the CARF domain that is specific to cA_6, the HEPN domain shows clear preference for RNA degradation (Figure 4A and Supplementary Figure S7A). However, at high cA_6 concentrations, HEPN domain also becomes a ring nuclease that effectively degrades cA_6 down to A_2>p and A>p (Figures 3E and 4C). Unlike the CARF ring nucleases that exhibit strict specificity and cleave either cA_6 or cA_4 oligoadenylates, the HEPN domain degrades all cA_ns, including cA_6, produced by the Csm effector complex (Figure 4C). It first opens the ring of cA_n and then chops linearized A_n>p like any other linear RNA (StCsm6 HEPN domain cuts linear RNA preferentially at AA or GA nucleotides (10)). Notably, an A>p molecule is bound to the HEPN domain in the structure of *T. onnurineus* Csm6 (25). The allosterically activated HEPN domain in StCsm6 is a much faster ring nuclease than the CARF domain (Figure 4B). The rate of cA_6 hydrolysis by the activated HEPN domain is similar to the cA_4 hydrolysis rate by the phage

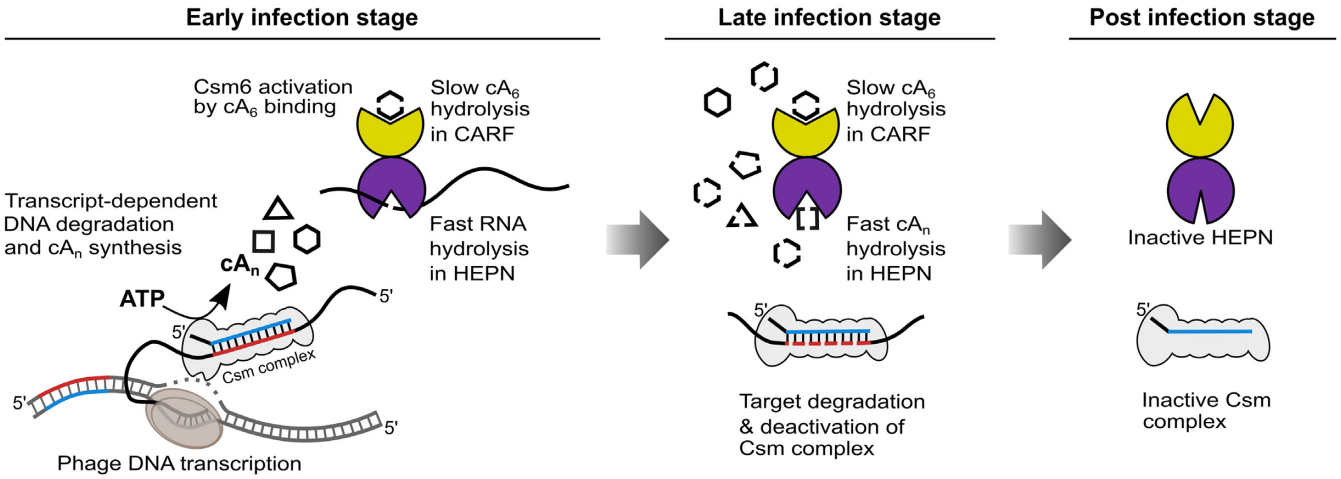

Figure 5. Model of self-regulation of the cA_n signaling pathway of type III-A CRISPR–Cas system. Recognition of the invasive transcript by the Csm complex triggers three catalytic activities: the Csm3-mediated cleavage of the invasive transcript, degradation of DNA template by the HD domain of Cas10, and synthesis of cA_{2-6} by the Palm domain of Cas10. The cA_6 acts as a signaling molecule that binds to the CARF domain of the Csm6 ribonuclease and activates non-specific RNA degradation by the HEPN domain. CARF domain acts as ring nuclease that slowly converts cA_6 into linear A_6>p and finally into A_3>p. Cleavage of the target RNA by Csm complex switches off cA_n synthesis by the Cas10 subunit. cA_6 and A_6>p remain bound to the CARF domain and activate the HEPN domain for degradation of cA_ns accumulated in the cell, thereby switching off signaling and restoring the pre-infection cell state.

ring nuclease, which is the fastest ring nuclease known to date and functions as viral anti-CRISPR (AcrIII-1) (26,50). During the preparation of the present manuscript, Foster *et al*. reported that *Pyrococcus furiosus* Csx1 HEPN is also capable of degrading cyclic oligoadenylates (51). It would be interesting to see if the allosterically activated HEPN domain degrades cA_ns in the cA_4-dependent CARF-HEPN nucleases (25,26,50) and whether majority of Csm6/Csx1 proteins are dual ring nucleases as StCsm6.

Csm6 as the regulator of type III-A CRISPR–Cas immunity

Our data and previous reports show that CARF-containing Csm6/Csx1 proteins play major role in the type III CRISPR–Cas immunity (46,52). Here we propose the following model of the type III-A Csm6-dependent CRISPR–Cas immunity (Figure 5). At an early infection stage, in response to the target RNA binding the Csm effector complex starts to produce cyclic oligoadenylates of various ring size. Cyclic hexa-adenylate cA_6 acts as a secondary messenger that allosterically activates Csm6 HEPN RNase through binding at the CARF domain and initiates RNA degradation. CARF domain also functions as a ring nuclease that slowly converts cA_6 to A_6>p and finally to A_3>p (Figure 3C). The slow turnover rate suggests that A_6>p remains bound to the CARF domain and may continue to activate the HEPN domain (11) until it is converted to A_3>p thereby switching off HEPN activity. This would provide a timer mechanism for the HEPN domain activity control.

The HEPN domain shows clear preference for RNA over cA_ns (Figure 4A and Supplementary Figure S7C) but can switch to cA_n degradation at high cyclic oligoadenylate concentration presumably at the late stage of phage infection. Notably, high concentrations of cA_5 and cA_6 (22.3 ± 4.6 and 12.9 ± 3.8 μM) are detected in *E. coli* harbouring the *S. thermophilus* type III-A CRISPR–Cas system and its target (Figure 2A).

E. coli is able to survive in the presence of cA_6-activated Csm6 RNase, which suggests that Csm6 does not degrade all cellular transcripts as its activity is self-regulated through the concerted action of CARF and HEPN ring nucleases (Figures 1C, 2C and 4). In the early infection stage, the activated Csm6 RNase could be co-localized with the Csm complex due to increased local concentration of cA_6, which is synthesized in response to target RNA binding. After cleavage of the foreign transcript at the late stage of infection, the cA_n synthesis is terminated (10,14) and accumulated cA_ns are degraded by cA_6-activated HEPN domain, thus completely eliminating the signaling molecules and switching off RNases (Figure 5). Such self-regulation mechanism would prevent the cell death and ensure the recovery of the host in the post-infection stage.

SUPPLEMENTARY DATA

Supplementary Data are available at NAR Online.

ACKNOWLEDGEMENTS

We thank Česlovas Venclovas for discussions and Giedrius Sasnauskas for critical reading of the manuscript and comments.

FUNDING

Research Council of Lithuania [MIP-40/2013, APP-3/2016 to G.T.]. Funding for open access charge: Research Council of Lithuania.

Conflict of interest statement. M. K., G.T. and V. S. are inventors on patent applications related to Csm complex. V. S. is a founder of CasZyme and a chairman of the board.

REFERENCES

1. Barrangou,R., Fremaux,C., Deveau,H., Richards,M., Boyaval,P., Moineau,S., Romero,D.A. and Horvath,P. (2007) CRISPR provides acquired resistance against viruses in prokaryotes. *Science*, **315**, 1709–1712.
2. Makarova,K.S., Wolf,Y.I., Iranzo,J., Shmakov,S.A., Alkhnbashi,O.S., Brouns,S.J.J., Charpentier,E., Cheng,D., Haft,D.H., Horvath,P. *et al.* (2020) Evolutionary classification of CRISPR–Cas systems: a burst of class 2 and derived variants. *Nature reviews. Microbiology*, **18**, 67–83.
3. Samai,P., Pyenson,N., Jiang,W., Goldberg,G.W., Hatoum-Aslan,A. and Marraffini,L.A. (2015) Co-transcriptional DNA and RNA cleavage during Type III CRISPR–Cas immunity. *Cell*, **161**, 1164–1174.
4. Tamulaitis,G., Venclovas,C. and Siksnys,V. (2017) Type III CRISPR–Cas immunity: major differences brushed aside. *Trends Microbiol.*, **25**, 49–61.
5. Elmore,J.R., Sheppard,N.F., Ramia,N., Deighan,T., Li,H., Terns,R.M. and Terns,M.P. (2016) Bipartite recognition of target RNAs activates DNA cleavage by the Type III-B CRISPR–Cas system. *Genes Dev.*, **30**, 447–459.
6. Estrella,M.A., Kuo,F.T. and Bailey,S. (2016) RNA-activated DNA cleavage by the Type III-B CRISPR–Cas effector complex. *Genes Dev.*, **30**, 460–470.
7. Han,W., Li,Y., Deng,L., Feng,M., Peng,W., Hallstrom,S., Zhang,J., Peng,N., Liang,Y.X., White,M.F. *et al.* (2017) A type III-B CRISPR–Cas effector complex mediating massive target DNA destruction. *Nucleic Acids Res.*, **45**, 1983–1993.
8. Kazlauskiene,M., Tamulaitis,G., Kostiuk,G., Venclovas,C. and Siksnys,V. (2016) Spatiotemporal control of Type III-A CRISPR–Cas immunity: coupling DNA degradation with the target RNA recognition. *Mol. Cell*, **62**, 295–306.
9. Liu,T.Y., Iavarone,A.T. and Doudna,J.A. (2017) RNA and DNA targeting by a reconstituted thermus thermophilus type III-A CRISPR–Cas system. *PLoS One*, **12**, e0170552.
10. Kazlauskiene,M., Kostiuk,G., Venclovas,C., Tamulaitis,G. and Siksnys,V. (2017) A cyclic oligonucleotide signaling pathway in type III CRISPR–Cas systems. *Science*, **357**, 605–609.
11. Niewoehner,O., Garcia-Doval,C., Rostol,J.T., Berk,C., Schwede,F., Bigler,L., Hall,J., Marraffini,L.A. and Jinek,M. (2017) Type III CRISPR–Cas systems produce cyclic oligoadenylate second messengers. *Nature*, **548**, 543–548.
12. Gruschow,S., Athukoralage,J.S., Graham,S., Hoogeboom,T. and White,M.F. (2019) Cyclic oligoadenylate signalling mediates Mycobacterium tuberculosis CRISPR defence. *Nucleic Acids Res.*, **47**, 9259–9270.
13. Han,W., Stella,S., Zhang,Y., Guo,T., Sulek,K., Peng-Lundgren,L., Montoya,G. and She,Q. (2018) A Type III-B Cmr effector complex catalyzes the synthesis of cyclic oligoadenylate second messengers by cooperative substrate binding. *Nucleic Acids Res.*, **46**, 10319–10330.
14. Rouillon,C., Athukoralage,J.S., Graham,S., Gruschow,S. and White,M.F. (2018) Control of cyclic oligoadenylate synthesis in a type III CRISPR system. *eLife*, **7**, e36734.
15. Nasef,M., Muffly,M.C., Beckman,A.B., Rowe,S.J., Walker,F.C., Hatoum-Aslan,A. and Dunkle,J.A. (2019) Regulation of cyclic oligoadenylate synthesis by the Staphylococcus epidermidis Cas10-Csm complex. *RNA*, **25**, 948–962.
16. Anantharaman,V., Makarova,K.S., Burroughs,A.M., Koonin,E.V. and Aravind,L. (2013) Comprehensive analysis of the HEPN superfamily: identification of novel roles in intra-genomic conflicts, defense, pathogenesis and RNA processing. *Biol. Direct*, **8**, 15.
17. Makarova,K.S., Anantharaman,V., Grishin,N.V., Koonin,E.V. and Aravind,L. (2014) CARF and WYL domains: ligand-binding regulators of prokaryotic defense systems. *Front. Genet.*, **5**, 102.
18. Makarova,K.S., Haft,D.H., Barrangou,R., Brouns,S.J., Charpentier,E., Horvath,P., Moineau,S., Mojica,F.J., Wolf,Y.I., Yakunin,A.F. *et al.* (2011) Evolution and classification of the CRISPR–Cas systems. *Nat. Rev. Microbiol.*, **9**, 467–477.
19. Jiang,W., Samai,P. and Marraffini,L.A. (2016) Degradation of phage transcripts by CRISPR-associated RNases enables type III CRISPR–Cas immunity. *Cell*, **164**, 710–721.
20. Rostol,J.T. and Marraffini,L.A. (2019) Non-specific degradation of transcripts promotes plasmid clearance during type III-A CRISPR–Cas immunity. *Nat. Microbiol.*, **4**, 656–662.
21. Shmakov,S.A., Makarova,K.S., Wolf,Y.I., Severinov,K.V. and Koonin,E.V. (2018) Systematic prediction of genes functionally linked to CRISPR–Cas systems by gene neighborhood analysis. *Proc. Natl. Acad. Sci. U.S.A.*, **115**, E5307–E5316.
22. Athukoralage,J.S., Rouillon,C., Graham,S., Gruschow,S. and White,M.F. (2018) Ring nucleases deactivate type III CRISPR ribonucleases by degrading cyclic oligoadenylate. *Nature*, **562**, 277–280.
23. Molina,R., Stella,S., Feng,M., Sofos,N., Jauniskis,V., Pozdnyakova,I., Lopez-Mendez,B., She,Q. and Montoya,G. (2019) Structure of Csx1-cOA4 complex reveals the basis of RNA decay in Type III-B CRISPR–Cas. *Nat. Commun.*, **10**, 4302.
24. Athukoralage,J.S., Graham,S., Gruschow,S., Rouillon,C. and White,M.F. (2019) A type III CRISPR ancillary ribonuclease degrades its cyclic oligoadenylate activator. *J. Mol. Biol.*, **431**, 2894–2899.
25. Jia,N., Jones,R., Yang,G., Ouerfelli,O. and Patel,D.J. (2019) CRISPR–Cas III-A Csm6 CARF domain is a ring nuclease triggering stepwise cA4 Cleavage with ApA>p formation terminating RNase activity. *Mol. Cell*, **75**, 944–956.
26. Athukoralage,J.S., McMahon,S.A., Zhang,C., Gruschow,S., Graham,S., Krupovic,M., Whitaker,R.J., Gloster,T.M. and White,M.F. (2020) An anti-CRISPR viral ring nuclease subverts type III CRISPR immunity. *Nature*, **577**, 572–575.
27. Tamulaitis,G., Kazlauskiene,M., Manakova,E., Venclovas,C., Nwokeoji,A.O., Dickman,M.J., Horvath,P. and Siksnys,V. (2014) Programmable RNA shredding by the type III-A CRISPR–Cas system of Streptococcus thermophilus. *Mol. Cell*, **56**, 506–517.
28. Mogila,I., Kazlauskiene,M., Valinskyte,S., Tamulaitiene,G., Tamulaitis,G. and Siksnys,V. (2019) Genetic dissection of the Type III-A CRISPR–Cas system Csm complex reveals roles of individual subunits. *Cell Rep.*, **26**, 2753–2765.
29. Zheng,L., Baumann,U. and Reymond,J.L. (2004) An efficient one-step site-directed and site-saturation mutagenesis protocol. *Nucleic Acids Res.*, **32**, e115.
30. Sajed,T., Marcu,A., Ramirez,M., Pon,A., Guo,A.C., Knox,C., Wilson,M., Grant,J.R., Djoumbou,Y. and Wishart,D.S. (2016) ECMDB 2.0: a richer resource for understanding the biochemistry of E. coli. *Nucleic Acids Res.*, **44**, D495–D501.
31. Altschul,S.F., Madden,T.L., Schaffer,A.A., Zhang,J., Zhang,Z., Miller,W. and Lipman,D.J. (1997) Gapped BLAST and PSI-BLAST: a new generation of protein database search programs. *Nucleic Acids Res.*, **25**, 3389–3402.
32. Corpet,F. (1988) Multiple sequence alignment with hierarchical clustering. *Nucleic Acids Res.*, **16**, 10881–10890.
33. Robert,X. and Gouet,P. (2014) Deciphering key features in protein structures with the new ENDscript server. *Nucleic Acids Res.*, **42**, W320–W324.
34. Lu,G. (1996) A WWW service system for automatic comparison of protein structures. *Protein Data Bank Q. Newslett.*, **78**, 10–11.
35. DeLano,W.L. (2002) Pymol: an open-source molecular graphics tool. *CCP4 Newsl. Protein Crystallogr.*, **40**, 82–92.
36. Yoshioka,K. (2002) KyPlot – a user-oriented tool for statistical data analysis and visualization. *CompStat*, **17**, 425–437.
37. Du,B., Ji,W., An,H., Shi,Y., Huang,Q., Cheng,Y., Fu,Q., Wang,H., Yan,Y. and Sun,J. (2014) Functional analysis of c-di-AMP phosphodiesterase, GdpP, in Streptococcus suis serotype 2. *Microbiol. Res.*, **169**, 749–758.
38. Huynh,T.N., Luo,S., Pensinger,D., Sauer,J.D., Tong,L. and Woodward,J.J. (2015) An HD-domain phosphodiesterase mediates cooperative hydrolysis of c-di-AMP to affect bacterial growth and virulence. *Proc. Natl. Acad. Sci. U.S.A.*, **112**, E747–E756.
39. Carte,J., Wang,R., Li,H., Terns,R.M. and Terns,M.P. (2008) Cas6 is an endoribonuclease that generates guide RNAs for invader defense in prokaryotes. *Genes Dev.*, **22**, 3489–3496.
40. Yang,W. (2011) Nucleases: diversity of structure, function and mechanism. *Q. Rev. Biophys.*, **44**, 1–93.
41. Makarova,K.S., Wolf,Y.I., Iranzo,J., Shmakov,S.A., Alkhnbashi,O.S., Brouns,S.J.J., Charpentier,E., Cheng,D., Haft,D.H., Horvath,P. *et al.* (2019) Evolutionary classification of CRISPR–Cas systems: a burst of class 2 and derived variants. *Nat. Rev. Microbiol.*, **18**, 67–83.
42. Whiteley,A.T., Eaglesham,J.B., de Oliveira Mann,C.C., Morehouse,B.R., Lowey,B., Nieminen,E.A., Danilchanka,O., King,D.S., Lee,A.S.Y., Mekalanos,J.J. *et al.* (2019) Bacterial

cGAS-like enzymes synthesize diverse nucleotide signals. *Nature*, **567**, 194–199.
43. Lau,R.K., Ye,Q., Birkholz,E.A., Berg,K.R., Patel,L., Mathews,I.T., Watrous,J.D., Ego,K., Whiteley,A.T., Lowey,B. *et al.* (2020) Structure and mechanism of a cyclic Trinucleotide-Activated bacterial endonuclease mediating bacteriophage immunity. *Mol. Cell*, **77**, 723–733.
44. Ye,Q., Lau,R.K., Mathews,I.T., Birkholz,E.A., Watrous,J.D., Azimi,C.S., Pogliano,J., Jain,M. and Corbett,K.D. (2019) HORMA domain proteins and a Trip13-like ATPase regulate bacterial cGAS-like enzymes to mediate bacteriophage immunity. *Mol. Cell*, **77**, 709–722.
45. Foster,K., Kalter,J., Woodside,W., Terns,R.M. and Terns,M.P. (2019) The ribonuclease activity of Csm6 is required for anti-plasmid immunity by Type III-A CRISPR–Cas systems. *RNA Biology*, **16**, 449–460.
46. Hatoum-Aslan,A., Maniv,I., Samai,P. and Marraffini,L.A. (2014) Genetic characterization of antiplasmid immunity through a type III-A CRISPR–Cas system. *J. Bacteriol.*, **196**, 310–317.
47. Meeske,A.J., Nakandakari-Higa,S. and Marraffini,L.A. (2019) Cas13-induced cellular dormancy prevents the rise of CRISPR-resistant bacteriophage. *Nature*, **570**, 241–245.
48. Abudayyeh,O.O., Gootenberg,J.S., Essletzbichler,P., Han,S., Joung,J., Belanto,J.J., Verdine,V., Cox,D.B.T., Kellner,M.J., Regev,A. *et al.* (2017) RNA targeting with CRISPR–Cas13. *Nature*, **550**, 280–284.
49. Garcia-Doval,C., Schwede,F., Berk,C., Rostol,J.T., Niewoehner,O., Tejero,O., Hall,J., Marraffini,L.A. and Jinek,M. (2020) Activation and self-inactivation mechanisms of the cyclic oligoadenylate-dependent CRISPR ribonuclease Csm6. *Nat. Commun.*, **11**, 1596.
50. Samolygo,A., Athukoralage,J.S., Graham,S. and White,M.F. (2020) Fuse to defuse: a self-limiting ribonuclease-ring nuclease fusion for type III CRISPR defence. *Nucleic Acids Res.*, **48**, 6149–6156.
51. Foster,K., Gruschow,S., Bailey,S., White,M.F. and Terns,M.P. (2020) Regulation of the RNA and DNA nuclease activities required for Pyrococcus furiosus Type III-B CRISPR–Cas immunity. *Nucleic Acids Res.*, **48**, 4418–4434.
52. Deng,L., Garrett,R.A., Shah,S.A., Peng,X. and She,Q. (2013) A novel interference mechanism by a type IIIB CRISPR-Cmr module in Sulfolobus. *Mol. Microbiol.*, **87**, 1088–1099.